Global Power and Propulsion Society
ISSN-Nr: 2504-4400
GPPS Xi'an21
18th-20th October 2021
www.gpps.global

GPPS-TC-2021-0354

NONLINEAR FLUTTER ANALYSIS OF THE ZERO NODAL DIAMETER OF A LABYRINTH SEAL

Roque Corral [*†], **Michele Greco and J. Luis Matabuena**
School of Aeronautics and Space
Universidad Politécnica de Madrid
28040 Madrid, Spain
e-mail: roque.corral@upm.es, michele.greco@upm.es

ABSTRACT

A non-linear reduced-order model has been used to assess the nonlinear stability of labyrinth seals in the case that circumferential variations are neglected. The model numerically solves the integral mass and energy equations of the seal for a prescribed motion until a periodic state is reached. For small vibration amplitudes, the work-per-cycle coincides with the one derived by Corral and Vega (2018, "Conceptual Flutter Analysis of Labyrinth Seals Using Analytical Models. Part I: Theoretical Background", ASME J. Turbomach. 140(10), pp. 121006) and Corral et al. (2021, "Higher-Order Conceptual Model for Seal Flutter", ASME J. Turbomach. 143(7), pp. 071006), but for large but still realistic vibration amplitudes nonlinearities alter the stability limit. If the seal is supported on the low-pressure side high vibration amplitudes tend to stabilise the seal even more. However, linearly stable seals supported on the high-pressure side can become unstable. Nonlinear effects are significant when the discharge time of the seal is comparable to the vibration period but for high enough frequencies nonlinear effects can be disregarded. This latter limit is the most realistic and therefore it is concluded that nonlinear mechanisms can play a significant role in seal flutter this is not the case for the zero nodal diameter under realistic conditions.

INTRODUCTION

Labyrinth seals are extensively used in aero-engines to control the leakage between regions with different pressures to prevent the ingestion of hot gas in the turbine disk cavities and for cooling operations (Chupp et al., 2006). They are comprised of rotating and stationary components. The rotating parts are usually equipped with a series of radial fins while the stationary elements have straight or stepped geometries. The flow is repeatedly forced to pass through small clearances generating kinetic energy that is dissipated in the inter-fin cavity. This process increases the resistance to flow compared to a smooth slot.

---

[*]Professor of Aerospace Engineering, Department of Fluid Mechanics and Aerospace Propulsion, Universidad Politécnica de Madrid
[†]corresponding author

The first pioneering studies on seal flutter were conducted during the 60' and 70' by Alford (1964; 1971; 1975). His works discuss the cause and prevention of fatigue failures in seals. He identified the importance of the support side of the seal in preventing self-excited vibration. Ehrich (1968) introduced the importance of the knife-edge clearance on the seal stability, but his findings were restricted to the 0th nodal diameter. Ehrich (1968) proposed an analytical model and identified a stability parameter that included the effect of the clearance, the support side of the seal and the geometry of the inter-fin cavity. The models described by Ehrich and Alford did not take into account the effect of the circumferential flow. Abbott (1981) found that a seal supported on the low-pressure side was unstable only if the mechanical frequency was lower than the acoustic frequency of the seal, and vice-versa. According to Abbott's criterion, the mechanical to acoustic frequency ratio and the support side of the seal are the only two parameters that control the stability of the seal.

All the previous studies were based on experimental analysis, failure evidence and often on bulk-flow analytical models. Nowadays, CFD analyses are commonplace both in industry and academia. Mare et *al.* (2010) conducted a parametric investigation on a multi-finned straight-through seal to investigate the influence of the frequency and the support location on the seal stability. They found that the aerodynamic damping depended mainly on the cavity shape, the mode-shape and the unsteady pressure phase distribution. Di Mare et al. (2010) describe the application of a time-marching nonlinear Navier-Stokes solver to the stability analysis of an LP turbine labyrinth seal for two different configurations. The results are compared with Abbott's stability criterion suggesting that complex seal configurations are not appropriate to be treated with simple stability criteria based on the comparison of the structural and acoustic frequencies. More recently, Miura and Sakai (2019) have compared CFD results with experimental data obtained in an in-vacuum rotating rig. The numerical results show reasonably good agreement with the measurements.

Recently, Corral and Vega proposed a new comprehensive model for seal flutter (Corral and Vega, 2018; Vega and Corral, 2018). The model provides an expression for the work-per-cycle involving two new and additional dimensionless parameters to define the stability map of the seal. All the results of the classical analytical models (Abbot, 1981; Ehrich, 1968) are recovered and conciliated. The results were also extended to stepped-seals Corral et al. (2020). Moreover, it has been identified that the tip labyrinth seal has an outstanding effect on the stability of shrouded turbine rotor blades Corral et al. (2019). The numerical results are compared with the prediction of the Corral and Vega (CV) model corroborating the stabilizing effect predicted analytically. Recently, a new formulation of the baseline Corral and Vega model (2018) accounting for non-isentropic perturbations has been proposed (Corral et al., 2021b). The model redefines the dimensionless parameters described in Corral and Vega (2018) and outlines a more general stability map of the seal. The high sensitivity of the seal stability to differential gapping, the role of the effective gaps and the carry-over coefficient, and thorough verification of the model using CFD have been addressed recently (Corral et al., 2021a).

Though the progress in the understanding of seal flutter in the last years has been huge thanks to the use of linearised analytical models, new dimensionless parameters, and simulations, the question of the impact of nonlinearities on the aeromechanic instability of labyrinth seals remains open. Labyrinth seals undergo extreme uncontrolled excursions through an engine mission. Seals rub or impact in the casing and the honeycomb, and in some instants the seal closures becomes zero or very small. Since the variations of the gaps concerning the nominal ones are and under these circumstances large, the flow variations within the inter-fin cavities are large and it can be expected that nonlinearities play an important role.

This paper explores the nonlinear aeromechanic stability of labyrinth seals on the zero nodal diameter for the sake of simplicity. Though the engineering interest of this mode is limited, it is important to understand first the impact of high vibration amplitudes in this case before moving to the higher nodal diameter cases. Firstly a reduced-order model is introduced and non-dimensionalised. Then the model is integrated numerically exploring the parameter space varying the vibration amplitude. Finally, some conclusions are drawn.

GOVERNING EQUATIONS

The model solves the integral form of mass of and energy equations for the inter-fin cavity volume per unit length in the circumferential direction, $V_{c,2D}$,

$$\frac{d}{\partial t}(\rho_c V_{c,2D}) = \dot{m}_1 - \dot{m}_2 \tag{1}$$

$$\frac{1}{\gamma - 1}\frac{d}{\partial t}(p_c V_{c,2D}) = \dot{m}_1 h_{0,1} - \dot{m}_2 h_{0,2} - p_c \frac{dV_{c,2D}}{dt} \tag{2}$$

where ρ_c and p_c are the spatially averaged fluid density, and static pressure in the cavity respectively, $V_{c,2D}$ is the volume per unitary span of the inter-fin cavity, and $\dot{m}_1$ and $\dot{m}_2$ represent the inlet and outlet mass flows, respectively (see Corral et al. (2021b) for the details of the derivation and Fig. 1 for a sketch of the seal geometry and the nomenclature). If the flow moves from the high-pressure side (HPS) to the low-pressure side (LPS) then $h_{0,1}$is the total enthalpy in the HPS cavity, $h_{0,1} = h_0$, and $h_{0,2}$ the spatially averaged total enthalpy

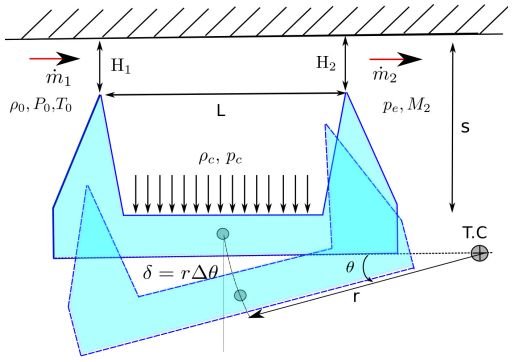

FIGURE 1. **Sketch of a simplified labyrinth and nomenclature**

in the cavity. Since the total enthalpy ingressed by the downstream gap comes either directly from the wall-jet or from the stagnated recirculation zone of the inter-fin cavity, in this work, it will be assumed that the total and static enthalpy of the cavity coincide, i.e. $h_{0,2} = h_c$. The momentum equation is not needed in this exploratory study since the circumferential variations are null for the zero-th nodal diameter.

For an ideal gas, the non-dimensional quasi-steady dimensionless mass-flows through the gaps, $\tilde{m}_1$, and $\tilde{m}_2$, can be expressed as a function of the ratio of the inlet total pressure, and the discharge static pressure, $\pi_i = P_{0,i}/p_i$, as:

$$\tilde{m}_1 = \frac{\dot{m}_1\sqrt{R_g T_0}}{P_0 A_1} = \pi_1^{-\frac{\gamma+1}{2\gamma}}\sqrt{\frac{2\gamma}{\gamma-1}\left(\pi_1^{\frac{\gamma-1}{\gamma}}-1\right)} = f(\pi_1), \text{ and } \tilde{m}_2 = \frac{\dot{m}_2\sqrt{R_g T_{0,c}}}{P_{0,c} A_2} = \pi_2^{-\frac{\gamma+1}{2\gamma}}\sqrt{\frac{2\gamma}{\gamma-1}\left(\pi_2^{\frac{\gamma-1}{\gamma}}-1\right)} = f(\pi_2) \tag{3}$$

where T_0, P_0, and $T_{0,c}(t)$, $P_{0,c}(t)$ are the inlet and the cavity spatially averaged total temperatures and pressures respectively. The dimensionless mass flows are a function only of the gap Mach number or the the pressure ratios $\pi_1 = P_0/p_c$ and $\pi_2 = P_{0c}/p_e$. The flow through the knife-seal is assumed quasi-stationary since the characteristic length of the inlet and outlet gaps of the inter-fin seal cavity, H_1 and H_2 respectively, and their thicknesses are much smaller than the characteristic size of the inter-fin cavity, L, and therefore the fin through-flow time is much smaller than the cavity discharge time. The wall heat flux in the seal is negligible and the process is adiabatic. Moreover, the work added by the seal rotation or the volume variation of the inter-fin cavity of the seal is negligible and therefore the mean total enthalpy in the inter-fin cavity is constant and equal to that of the inlet, even for large variations of the seal gaps.

The volume, $V_{c,2D}(t)$, and the gaps,$A_1(t)$ and $A_2(t)$, of the seal undergo an harmonic variation of angular velocity ω which are directly related with the mode-shape. Using the following dimensionless variables

$$\tilde{\rho}_c = \frac{\rho_c}{\rho_0}, \tilde{p}_c = \frac{p_c}{P_0}, \tilde{V}_{c,2D} = \frac{V_{c,2D}}{V_{c,0}}, \tilde{A}_j = \frac{A_j}{A_0}, \tau = \omega t \tag{4}$$

the non-dimensional continuity and energy equations become

$$\frac{1}{\gamma}\Omega_{NL}\frac{d}{d\tau}(\tilde{\rho}_c\tilde{V}_{c,2D}) = \tilde{A}_1(\tau)f(\tilde{p}_c) - \tilde{A}_2(\tau)\tilde{p}_c f(\tilde{p}_c\pi_T) \tag{5}$$

$$\Omega_{NL}\frac{d}{d\tau}(\tilde{p}_c\tilde{V}_{c,2D}) = \tilde{A}_1(\tau)f(\tilde{p}_c) - \tilde{A}_2(\tau)\tilde{p}_c^2\tilde{\rho}_c^{-1}f(\tilde{p}_c\pi_T) - (\gamma-1)\Omega_{NL}\tilde{p}_c\frac{d\tilde{V}_{c,2D}}{d\tau} \tag{6}$$

where the dimensionless parameter

$$\Omega_{NL} = \omega\frac{P_0 V_{c,0}}{\dot{m}_c a_0^2} \tag{7}$$

represents the ratio of the seal discharge time through the gaps $t_d = P_0 V_{c,0}/(m_c a_0^2)$ and the vibration period of the seal. Unlike in the linear problem, the total intlet temperature and pressure are used to construct this dimensionless parameter instead the mean static pressure and temperature. In this context, the characteristic mass-flow is $\dot{m}_c = P_0 A_0/\sqrt{R_g T_0}$. If the seal is deemed to move as a rigid body in the meridional section of the seal, the gap and volume time variations can be expressed as function of the distance to the pivot centre, r, considered positive if it is located in the LPS, the geometry of the seal L, s, and H_0 and the vibration amplitude, $\Delta\theta$, as:

$$\tilde{A}_{1,2} = 1 + \frac{r \pm L/2}{H_0}\Delta\theta\sin\tau, \text{ and } \tilde{V}_{c,2D} = 1 + \frac{r}{s}\Delta\theta\sin\tau. \tag{8}$$

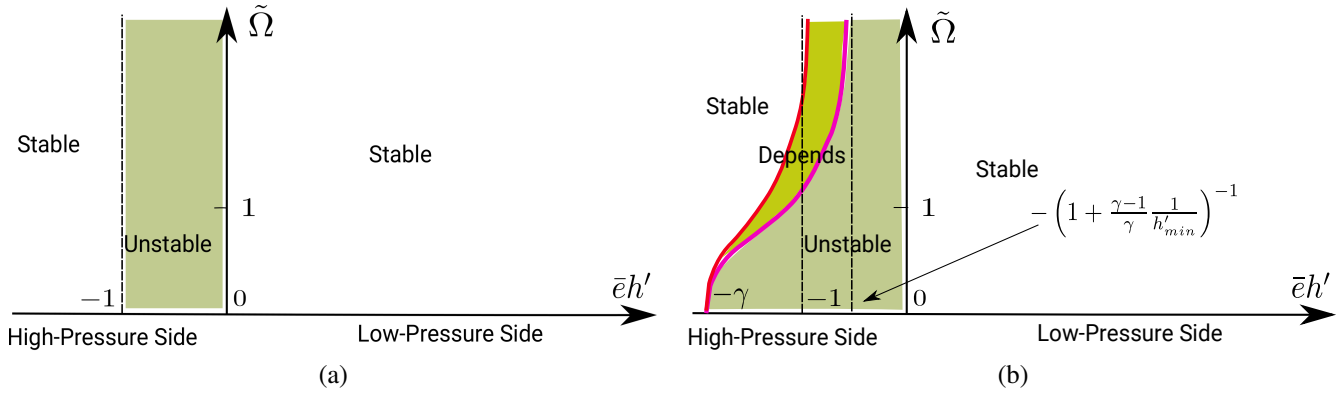

FIGURE 2. **Stability region of the 0^{th} nodal diameter according to Ehrich (1968) and the baseline Corral & Vega model (Corral and Vega, 2018; Vega and Corral, 2018) (a) and the higher-order CV model (Corral et al., 2021b)(b) as a function of the dimensionles distance from the pivot center of the mode to the seal mid-point ($\tilde{e}h'$) and the dimensionless frequency ($\tilde{\Omega}$).**

LINEAR SOLUTION

The main results concerning the linearized model of a seal vibrating without circumferential variations (the so-called zero nodal diameter) are summarized here for the sake of completeness and ease the discussion and comparison with the nonlinear results in the limit of small vibration amplitudes. It is important to remark that the linear model has been extensively compared with linearized 3D Navier-Stokes solutions delivering always excellent results. The largest sets of comparisons can be found in Corral and Greco (2021) for the 0th ND, and in Corral et al. (2021a) for other modes and dissimilar gaps.

The linearised model gives the dimensionless critical frequency, $\tilde{\Omega} = \Omega/h'$, as function of the dimensionles distance of the pivot centre

$$\tilde{e}h' = \gamma \frac{rH}{sL} h' \tag{9}$$

where $h'$is a fucnction of the total pressure ratio of the seal (see appendix A in Corral and Vega (2018)). The actual values of $\tilde{\Omega}$ and $\tilde{e}h'$ are more involved in the non-isentropic model but the details (see Corral et al. (2021b)) are not necessary here to follow the discussion.

Figure 2 (a) illustrates the CV stability criterion derived in (Corral and Vega, 2018) for isentropic perturbations, which matches the Ehrich's criterion (Ehrich, 1968) if it is properly non-dimensionalized. The main idea is that the stability of the 0th ND depends solely on the position of the torsion centre and not on the frequency. Seals supported on the LPS are always stable whereas those supported on the HPS are unstable if the pivot centre is close to the seal but when the pivot centre is located far away the stability is recovered. This limit in non-dimensional terms occurs at $\tilde{e}h' = -1$.

When the flow is not deemed isentropic and the energy equation is retained Corral et al. (2021a), seals supported on the LPS are always stable again but there is a significant region on the HPS where the stability depends on the frequency and the pressure ratio of the seal because $\tilde{e}h'_{eff}$ is a function of $\tilde{\Omega}$ (see Fig. 2 (b)). In other words, the simple stability criterion yielded by the baseline CV model becomes more complex on the HPS. The main difference with respect the baseline CV model is that the unstable region is enlarged when the non-dimensional frequency is lowered. Moreover, the critical values of $\tilde{e}h'$ in the HPS which mark the change of stability depend on the pressure ratio. When $\Omega \to \infty$ the stability limit curves (depicted in red) are obtained between $\tilde{e}h' = -1$, for very low-pressure ratios, and $\tilde{e}h' = \tilde{e}h'^{*} - (1+(\gamma-1)/(\gamma h'_{min}))^{-1}$, for choked seals. For very low frequencies, the critical value tends to $\tilde{e}h' = -\gamma$, independently of the seal pressure ratio.

Many concludions have been drawn from the linear CV model, one of the most usefiul is the correct scaling of the work-per-cycle. The dimensionless work-per-cycle is defined as

$$\tilde{W}_{cyc} = \frac{W_{cyc}}{\pi p_{c,s} \delta^2 SL/|r|H_0 h'} \tag{10}$$

where $S = 2\pi RL$ is the surface of the land seal, $p_{c,s}$the mean pressure of the inter-fin cavity, r the distance of the pivot point to the mid-point of the seal and $\delta = r\Delta\theta$, the vibration amplitude of the mid-point point of the seal.

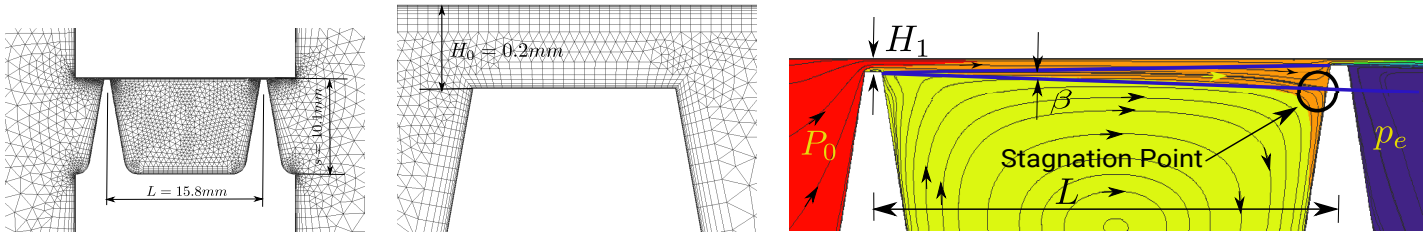

(a) (b) (c)

FIGURE 3. **Details of the labyrinth seal used in the present study. A: Inter-fin cavity region. B: Tip clearance region. C: Sketech of the steady-state flow in the inter-fin cavite. (Cavity Radius (R) 554 mm, nominal gap $H = 0.2$ mm, height $s = 10.1$ mm, and length $L = 15.8$ mm.)**

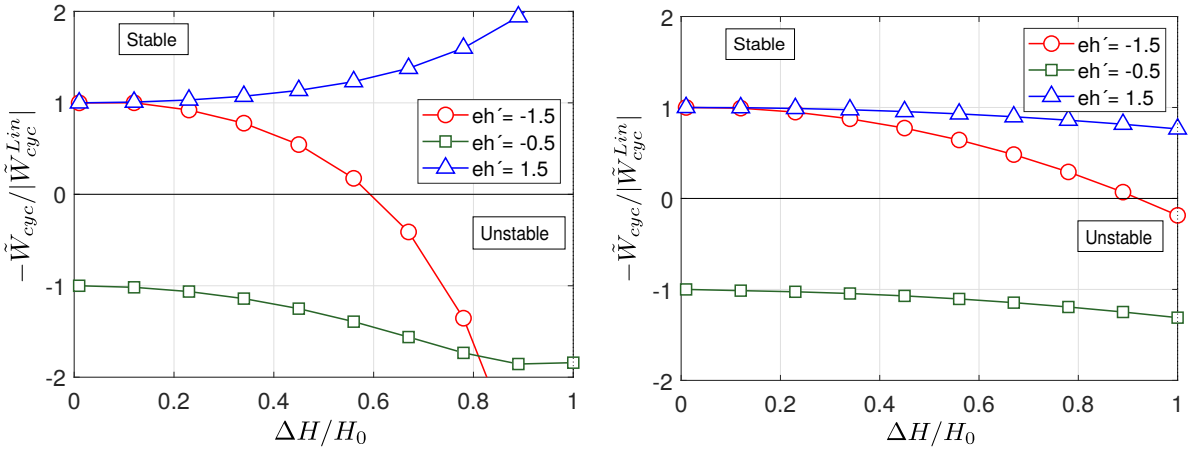

(a) Ω=1.2 (b) Ω=24

FIGURE 4. **Dimensionless work-per-cycle variation normalised with the work-per-cycle of the linear (small amplitude) case as a function of the vibration amplitude for different positions of the dimensionless torsion center ($\tilde{e}h'$). The total pressure ratio of the seal is $\pi_T = P_0/p_e$=1.2 and the corresponding $h' = 10.5$.**

NUMERICAL MODEL

Equations 1 and 2 are integrated in time using a fourth-order Runge-Kutta for a prescribed harmonic motion until the solution converges to a periodic state. The work-per-cycle is extracted from the last cycle of the converged solution. The geometry used to explore the nonlinearity of the model has been used in previous works Corral and Greco (2021); Corral et al. (2021a) and is sketched in Fig. 3. The simplified geometry consists of a two-fin straight-through seal for which the linear model reproduced the results obtained with a three-dimensional linearized Navier-Stokes solver.

Figure 3c outlines the steady-state flow that can be seen in the inter-fin cavity region of a labyrinth seal. Essentially the high-speed wall-jet created in the inlet gap impinges in the downstream fin at the same time that a large low-speed recirculation bubble which essentially uniform static pressure is created.

RESULTS

Figure 4 shows the variation of the dimensionless work-per-cyce of the seal, $\tilde{W}_{cyc}$, as a function of the vibration amplitude of the seal ($\Delta H/H_0$) and the dimensionless frequency ($\tilde{\Omega}$) normalised with the small amplitude (linear) limit, $\tilde{W}^{Lin}_{cyc}$, which is obtained when $\Delta H/H_0 \to 0$. When $\Delta H/H_0 = 1$ the tip of the seal fin rubs with the static part during a single instant of the vibration period. It is important to remark that ΔH is the clearance variation of the fin tip located farther away from the pivot centre. If the seal is supported on the LPS this vibration amplitude corresponds to the tip of the inlet fin whereas if the seal is supported on the HPS this amplitude is that of the exit fin. Two dimensionless frequencies $\Omega = 1.2$ and 24 are presented being the former too low for a realistic case while the

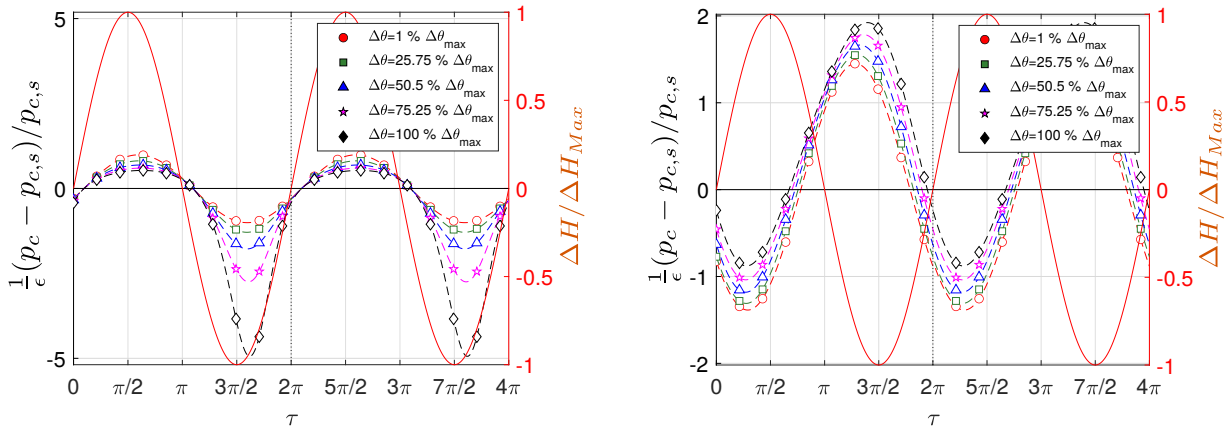

(A) $\Omega = 1.2$ (B) $\Omega = 24$

FIGURE 5. **Impact of the clearance on the unsteady pressure time signal for two different frequencies for a seal supported on LPS** ($\tilde{e}h' = +1.5$,$\pi_T = 1.2$, $h' = 10.5$)

latter is deemed representative. The geometric parameters of the two-fin straight through seal used in this work are clearance $H = 0.2$ mm, height $s = 10.1$ mm, and length $L = 15.8$.

The first remark is that the quadratic dependence of work-per-cycle with the vibration amplitude which is obtained from the linear analysis, i.e. $\tilde{W}_{cyc}^{Lin} \propto \delta^2 \propto (\Delta H)^2$, is already removed from the plot so the variation of $\tilde{W}_{cyc}$ with the amplitude shown in Fig. 4 is due to higher-order terms. It can be observed that for the cases displayed here, the linear behaviour holds as long as $\Delta H/H_0 \ll 1$ which is an expected result. In practice, for $\Delta H/H_0 \simeq 0.2$ the seal behaves still linearly but for higher values of the amplitude, the seal can change the character of the stability. Stable seals supported on the HPS ($\tilde{e}h' = -1.5$) can become unstable but seemingly stable seals supported in the LPS become more stable though from Fig. 4 the opposite trend is observed. The main conclusion is that nonlinearities can play an important role in realistic situations.

Another important conclusion is that since the nonlinear correction to the work-per-cicle scales as δ^4, i.e. $W_{cyc} = \bar{W}_{cyc}^{Lin}\delta^2 + \bar{W}_{cyc}^{NL}\delta^4$ the dimensionless W_{cyc} renormalised with the linear work-per-cycle is

$$\frac{W_{cyc}}{W_{cyc}^{Lin}} = 1 + \frac{\bar{W}_{cyc}^{NL}}{\bar{W}_{cyc}^{Lin}}\delta^2 \tag{11}$$

and the curves displayed in Fig. 4 are parabolas (at least for $\Delta H/H_0 \ll 1$).

The comparison of Figs. 4a and 4b leads to the conclusion that nonlinear effects are stronger at low frequencies than at high frequencies. This fact can be corroborated by looking at the static pressure time signals of the final periodic state displayed in Fig. 5. The unsteady pressure is renormalised with the linear estimate of the unsteady pressure derived in Corral and Vega (2018) where it was found that $p_c' = (p_c - p_{c,s}) \sim \varepsilon p_{c,s}$ with $\varepsilon = L\Delta\theta/(H_0 h')$, and which for small amplitudes is small necessarily.

The seal is supported on the LPS ($\tilde{e}h' = +1.5$) and Fig. 4a shows that the closing and opening intervals of the seal behave in a completely different manner being the former highly nonlinear for large vibration amplitudes. The unsteady pressure amplitude grows higher than linear with the vibration amplitude for high vibration amplitudes. Moreover, it can be noticed that the mean value of the static pressure in the inter-fin cavity experiences a drift from the steady-state value due to nonlinear effects. This is another indication of the non-linearity of the problem.

The situation is quite different at high-frequencies (precisely speaking $\Omega \gg 1$). Figure 4b shows that the unsteady pressure has a sinusoidal shape for $\Omega = 24$ which is an indication of the linearity of the problem. However, the mean pressure changes with the vibration amplitude.

The quasi-linear sinusoidal behaviour of the unsteady pressure is the result of two combined effects, namely the high frequency and the fact that the volume variations of the inter-fin cavity are small compared to the volume. The dimensionless volume $\tilde{V}_{c,2D} = 1 + \tilde{v}_c \sin\tau$ where $\tilde{v}_c = \delta/s < H_0/s \ll 1$. The dimensionless mass and energy equations are of the form

$$\frac{d}{d\tau}(\tilde{\rho}_c \tilde{V}_{c,2D}) = \frac{1}{\Omega_{NL}} F_m(\tilde{\rho}_c, \tilde{p}_c, \tau) \simeq 0, \text{ and } \frac{d}{d\tau}(\tilde{p}_c \tilde{V}_{c,2D}) - (\gamma - 1)\tilde{p}_c \frac{d\tilde{V}_{c,2D}}{d\tau} = \frac{1}{\Omega_{NL}} F_e(\tilde{\rho}_c, \tilde{p}_c, \tau) \simeq 0 \tag{12}$$

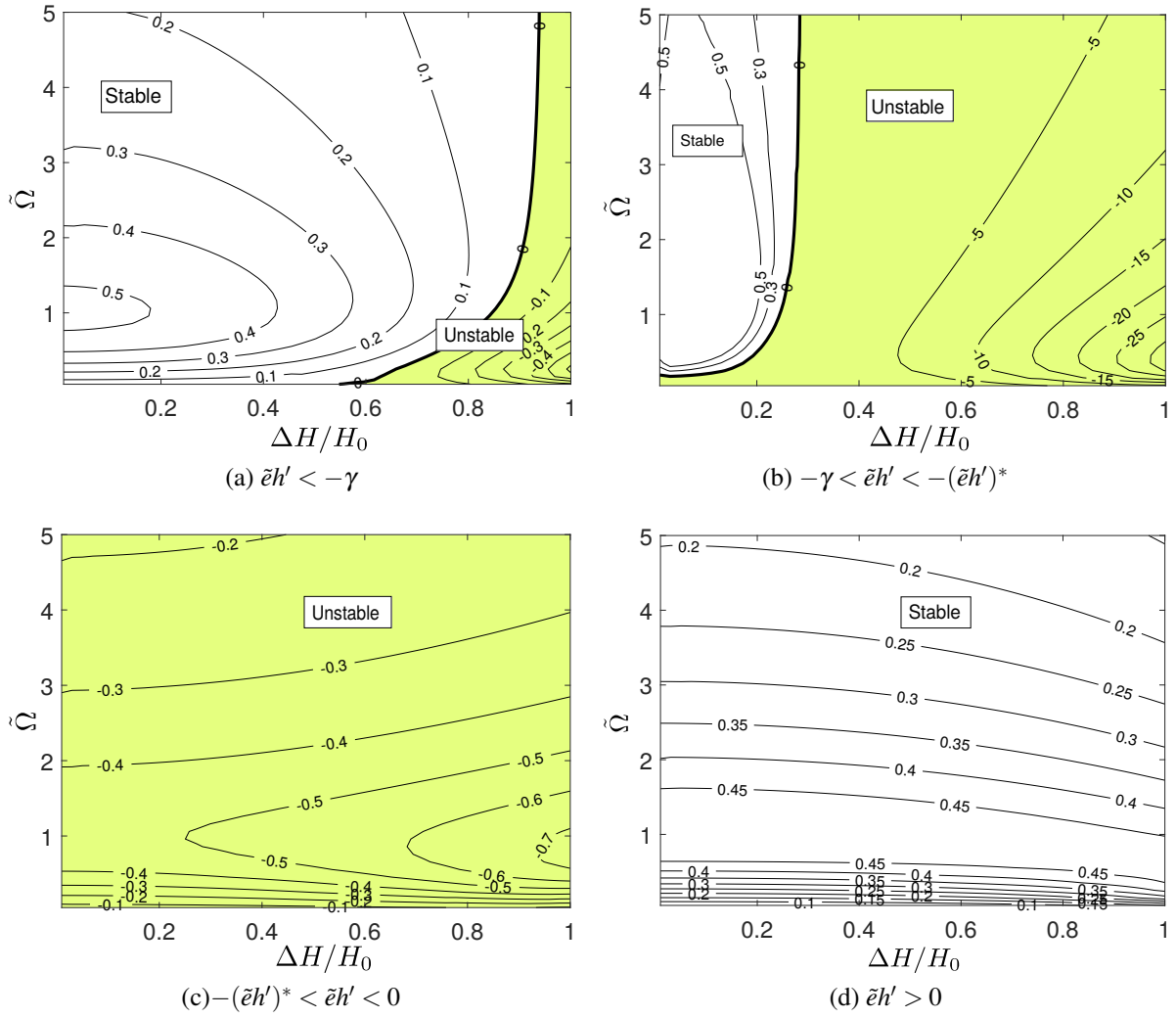

(a) $\tilde{e}h' < -\gamma$ (b) $-\gamma < \tilde{e}h' < -(\tilde{e}h')^*$

(c) $-(\tilde{e}h')^* < \tilde{e}h' < 0$ (d) $\tilde{e}h' > 0$

FIGURE 6. **Dimensionless work-per-cycle over $|1+\tilde{e}h'|$ as a function of the vibration amplitude ($\Delta H/H_0$) and the dimensionless frequency ($\tilde{\Omega} = \Omega/h'$) for different positions of the dimensionless torsion centre. Shaded regions denote unstable seals.**

where F_m and F_e are nonlinear functions whose impact is negligible in first approximation if $\Omega_{NL} \gg 1$. The mass equation neglecting terms small terms of the form $\mathcal{O}(\tilde{v}_c)$ and $\mathcal{O}(\Omega_{NL}^{-1})$ can be written as

$$\frac{d\tilde{\rho}_c}{d\tau} + \tilde{\rho}_c \tilde{v}_c \cos\tau \simeq 0 \tag{13}$$

whose periodic solution is $\tilde{\rho}_c/\tilde{\rho}_{c,s} = e^{-\tilde{v}_c \sin\tau} \simeq 1 - \tilde{v}_c \sin\tau$. Analogously, the energy equation reduces in first approximation to $\tilde{p}_c/\tilde{p}_{c,s} \simeq 1 - \gamma\tilde{v}_c \sin\tau$. Therefore, the unsteady perturbations at high frequency are isentropic, as it had already been observed in Corral et al. (2021b), and harmonic in first approximation.

Figure 6 displays the isolines of $\tilde{W}_{cyc}/|1+\tilde{e}h'|$ as a function of $\tilde{\Omega}$ and the vibration amplitude for four different characteristic positions of the dimensionless torsion radius $\tilde{e}h'$. The first case corresponds to pivot centres located on the LPS (Fig. 6d represents the case $\tilde{e}h' = 1.5$) which are always stable independently of the frequency and the vibration amplitude. In this case, the linear and nonlinear stability limits (Fig. 2b) are identical.

The rest of the cases are associated with pivot points located on the HPS. If the pivot point is located far away from the seal mid-point, $\tilde{e}h' < -\gamma$, the seal is stable according with the linear criterion but for high enough vibration amplitudes the seal becomes unstable. Figure 2 presents the results for $\tilde{e}h' = -1.5$. For pivot points closer to seal mid-point and in the range $-\gamma < \tilde{e}h' < -(\tilde{e}h')^*$, where the

critical value of the dimensionless torsion centre is $(\tilde{e}h')^* = (1+\frac{\gamma-1}{2}h'^{-1}_{min})^{-1}$, the stability of the zero ND depends on the frequency and the pressure ratio according with the linear stability criterion (see Fig. 2). The results displayed in Fig. 6b for $\tilde{e}h' = -1$ show that the stability depends as well on the vibration amplitude.

Finally, pivot points located on the HPS but close to the mid-point of the seal in the range $-(\tilde{e}h')^* < \tilde{e}h' < 0$, are always unstable according to both the linear and nonlinear predictions. Fig. 6c shows the results for the case $\tilde{e}h' = -0.5$. It is worth noting that for all the cases the maximum work-per-cycle is obtained around $\tilde{\Omega} \simeq 1$ as it was predicted by the linear theory (Corral and Vega, 2018; Corral et al., 2021b).

Similar analysis have been carried out for higher pressure ratios (π_T=2.35 and 3.0), but surprisingly the conclusions are the same as the ones outlined for π_T=1.2 despite the fact that the exit gap can choke and unchoke during a vibration period (π_T=2.35) or remain choked during the whole oscillation (π_T=3.0). The results are not presented here for the sake of brevity.

CONCLUDING REMARKS

The nonlinear aeroelastic stability of labyrinth seals in the absence of circumferential variations has been assessed extending the use of a high-order linear model to the nonlinear regime. The expected accuracy of the results is high based on the precedents of the model.

The main conclusion is that in the presence of finite vibration amplitudes the linear stability threshold is altered when the seal is supported on the high-pressure side whereas if the seal is supported on the low-pressure side the seal is always stable. The vibration frequency plays a major role in the severity of nonlinear effects. Actually, for high enough vibration amplitudes nonlinear effects are small even if the vibration amplitude of the seal is high and the seal closure becomes zero. This result is justified by simplifying the model for the high-frequency limit. Moreover, nonlinear effects are weakly affected by the seal pressure ratio.

For practical cases in which the vibration frequency is much higher than the discharge time of the seal, the effect of nonlinearities on the zero nodal diameter is expected to be low but non-linear effects are expected to be high for other nodal diameters.

ACKNOWLEDGMENTS

This research work has been partially supported by the European project ARIAS, H2020 research and innovation program under grant agreement No. 769346. The authors gratefully acknowledge the financial support.

NOMENCLATURE

a_0	Speed of sound in the cavity
CV	Corral and Vega (2018) Model
h'	Seal pressure function
H	Fin clearance
HPS	High-Pressure Side
L	Seal cavity length
LPS	Low-Pressure Side
$\dot{m}$	Mass flow rate
$\dot{m}_{id}$	$= \frac{P_{0i}A_i}{\sqrt{RT}}\pi_i^{-(\gamma+1)/2\gamma}\sqrt{\frac{2\gamma}{\gamma-1}(\pi_i^{(\gamma-1)/\gamma}-1)}$ Ideal mass flow rate
ND	Nodal diameter
p_c	Cavity static pressure
p_e	Exit static pressure
P_0	Inlet total pressure
r	Torsion center position
R	Cavity radius
s	Cavity height
St	Vibration-to-acoustic frequency ratio
t_d	$= \frac{p_{c,s}V_{c,s}}{\dot{m}_s a_0^2}$. Seal cavity discharge time
W_{cyc}	Work per cycle

Greek symbols

γ	Heat capacity ratio
π_T	$= P_0/p_e$. Total pressure ratio
ω	Vibration angular frequency (rad/s)
Ω	$=\omega t_d$ Non-dimensional discharge time
$\Delta\theta$	Rotation angle
τ	Non-dimensional time

Super-scripts

˜	Non-dimensional values
’	Time perturbation

Sub-scripts

c	Cavity
cyc	cycle
e	Exit
s	Steady state

References

Abbot, D.R., 1981. Advances in labyrinth seal aeroelastic instability prediction and prevention. ASME J. Eng. Gas Turbines Power 103, 308–312.

Alford, J., 1964. Protection of labyrinth seals from flexural vibration. ASME J. Eng. Gas Turbines Power 86, 141–147.

Alford, J.S., 1971. Labyrinth seal designs have benefitted from development and service experience, in: SAE Technical Paper, SAE International. p. 710435. doi:10.4271/710435.

Alford, J.S., 1975. Nature, causes and prevention of labyrinth air seal failures. AIAA Journal of Aircraft 12, 313–318.

Chupp, R., Hendricks, R., Lattime, S., Steinetz, B., 2006. Sealing in turbomachinery. AIAA Journal of Propulsion and Power 22, 314–349. doi:https://doi.org/10.2514/1.17778.

Corral, R., Greco, M., 2021. Numerical validation of an analytical seal flutter model. Accepted in GPPS Journal .

Corral, R., Greco, M., Vega, A., 2019. Tip-shroud labyrinth seal impact on the flutter stability of turbine rotor blades. ASME J. of Turbomachinery 141, 101006. doi:10.1115/1.4043962.

Corral, R., Greco, M., Vega, A., 2021a. Effective clearance and differential gapping impact on seal flutter modelling and validation. Accepted in ASME J. Turbomach. .

Corral, R., Greco, M., Vega, A., 2021b. Higher-order conceptual model for seal flutter. ASME J. of Turbomachinery 143, 071006. doi:10.1115/1.4050334.

Corral, R., Vega, A., 2018. Conceptual flutter analysis of labyrinth seals using analytical models. part I: Theoretical background. ASME J. Turbomach. 140, 121006. doi:10.1115/1.4041373.

Corral, R., Vega, A., Greco, M., 2020. Conceptual flutter analysis of stepped seals. ASME J. Eng. Gas Turbines Power 142, 071001.

Ehrich, F., 1968. Aeroelastic instability in labyrinth seals. ASME J. Eng. Gas Turbines Power 90, 369–374.

Mare, L.D., Imregun, M., Green, J., Sayma, A.I., 2010. A numerical study on labyrinth seal flutter. ASME J Tribology 132, 022201–7.

Miura, T., Sakai, N., 2019. Numerical and experimental studies of labyrinth seal aeroelastic instability. ASME J. Eng. Gas Turbines Power 141, 111005. doi:doi.org/10.1115/1.4044353.

Vega, A., Corral, R., 2018. Conceptual flutter analysis of labyrinth seals using analytical models. Part II: Physical interpretation. ASME J. Turbomach. 140, 121007. doi:10.1115/1.4041377.